Peer Reviewed Review **open**access

Comprehensive review on land use/land cover change classification in remote sensing

M. Sam Navin and L. Agilandeeswari*

School of Information and Technology, Vellore Institute of Technology, Vellore, India

Contact

L. Agilandeeswari: agila.l@vit.ac.in
https://orcid.org/0000-0001-6147-9535

M.S. Navin: samnavin.m2018@vitstudent.ac.in
https://orcid.org/0000-0001-9068-1855

Research in the field of remote sensing of the environment is valuable and informative. Hyperspectral (HSP) and multispectral (MSP) satellite images have been used for different remote sensing applications. Land Use/Land Cover (LU/LC) change classification has been considered as important research in the field of remote sensing environment. This review aims to identify the various LU/LC applications, remote sensing satellites, geospatial software, pre-processing techniques, LU/LC classification, clustering, spectral unmixing, landscape change models and evaluation metrics. The main objective of this review is to present the more frequently used techniques for analysing LU/LC change with MSP and HSP satellite images. An aim of this review is to motivate future researchers to work efficiently with MSP and HSP satellite images in the field of remote sensing.

Keywords: remote sensing, hyperspectral and multispectral satellite images, image classification, land use/land cover change

Introduction

Analysing multispectral (MSP) and hyperspectral (HSP) satellite images in the field of remote sensing and the geographic information system (GIS) environment have become some of the hottest topics among researchers around the world. Everyday changes on the Earth's surface have a significant impact on society, and this has been the driver for researchers to work on the land use/land cover (LU/LC) change problem. The information gathered from various satellites has been used by researchers to map the Earth's features and infrastructures. Land use and land cover are two different terms to describe the Earth's surface. The land cover area represents the forest-covered areas, wetlands, grasslands, water-covered areas, mountainous regions and deserts etc. Specific events and changes that take place in land cover represent changes in land use categories, such as urbanisation, shopping centres, reservoirs and parks etc.[1] Observing the specific LU/LC changes that take place on the Earth's surface has been a significant problem for researchers. Time series satellite images have been acquired and analysed through various stages of LU/LC, namely pre-processing, classification and prediction, to solve the LU/LC change detection problem.[2]

Correspondence
L. Agilandeeswari (agila.l@vit.ac.in)

Received: 16 October 2019
Revised: 17 June 2020
Accepted: 13 July 2020
Publication: 2020
doi: 10.1255/jsi.2020.a8
ISSN: 2040-4565

Citation
M. Sam Navin and L. Agilandeeswari, "Comprehensive review on land use/land cover change classification in remote sensing", *J. Spectral Imaging* **9**, a8 (2020). https://doi.org/10.1255/jsi.2020.a8

A thematic representation of the LU/LC map with classified classes is considered an essential tool in visualising LU/LC changes in the study area.[3] Researchers use supervised and unsupervised machine learning algorithms to classify satellite images. Unsupervised, or clustering methods, include Fuzzy C Means clustering, Iterative Self-Organising Data Analysis (ISODATA) clustering, K-Means and Self-Organising Map (SOM) neural networks. Supervised, or classification, methods include Random Forest Classifiers (RFC), Support Vector Machines (SVM), k-Nearest Neighbour (kNN), Maximum Likelihood Classifier (MLC), Mahalanobis Distance Classifier, Parallelepiped Classifier and Minimum-Distance Classifier.[4] The LU/LC change prediction for a particular region or locality helps government officials, urban planners and forest departments to take the appropriate action to protect the land cover environment. Landscape simulation models include GIS, machine learning and hybrid models. GIS models include Slope, Land use, Exclusion, Urban extension, Transportation and Hill shade (SLEUTH), Conversion of Land Use and its Effects (CLUE), State and Transition Simulation Model (STSM), GeoMod, Landscape Disturbance and Succession (LANDIS), Spatially Explicit Landscape Event Simulation (SELES), Land Change Modeller (LCM) and LTM (Land Transformation Model). Machine learning models include Cellular Automata (CA), Linear Regression (LR), SVR (Support Vector Regression), Logistic Regression, Markov Chain, Box–Jenkins, Artificial Neural Network (ANN) and Random Forest (RF). Deep learning and boosting were also considered as a sub-field of the machine learning model. Many researchers have used hybrid models to predict LU/LC changes, including Multilayer Perceptron-Markov Chain (MLP-MC), Regression Tree-CA, CLUE-MC, CA-MC, ANN-CA and LR-MC.[5,6]

LU/LC change analysis in the field of remote sensing has been studied and observed by many researchers around the world. Time series LU/LC analysis of the Zagros forest was observed between 1992 and 2016 using MSP satellite images. The authors used pre-processing techniques, such as atmospheric and geometric corrections, to correct the noise present in the satellite images. The MSP satellite images were classified into forest, rangeland, agriculture and built-up areas with the MLC algorithm. The MLP neural network was used to calibrate the non-linear relationship between the explanatory variables. In order to analyse the LU/LC change, researchers used the MC model to compute the transition probability between the LU/LC maps of 2002 and 2012.[6]

Continuous classification of LU/LC changes using MSP satellite data of the Qingliu River catchment in southeast China was achieved with the Continuous Change Detection and Classification (CCDC) algorithm. The correlation between forest coverage and climatic factors was determined by calculating the Enhanced Vegetation Index (EVI). Use of the RFC method resulted in higher classification accuracy.[8]

MSP satellite images of the Hugumburda national forest priority area were acquired during 1985, 2000 and 2015. Digital Elevation Model (DEM) data from the Advanced Spaceborne Thermal Emission and Reflection Radiometer (ASTER) were acquired and used to derive topographic variables like slope, elevation and aspect. The authors validated the accuracy of the MLC by using Google Earth images and data from the Ethiopian Mapping Agency.[9] The Classification and Regression Tree (CART) method was used for processing and analysing the satellite images. Change-vector analysis in posterior probability space was used to evaluate the characteristics of the satellite images over different periods. For LU/LC change detection, the Histogram Maximum Entropy method was used. The Normalised Difference Vegetation Index (NDVI) measures the annual coverage of vegetation on Earth.[10] The LU/LC change at Shirgah, in northern Iran, was analysed by Multivariate Adaptive Regression Spline (MARS), CART and RF classification techniques. The post-classification performed to validate the classified images gave accurate results.[11] Pixel, subpixel and object-based classification methods are used to produce a thematic map of different time-series data. An accuracy assessment was performed to validate the detailed LU/LC map against reference or ground truth data.[1,3,4,6–57] CA and Markov Chain Analysis are the most used hybrid models for monitoring features that change in time and space.[6,22–27,31,33,53,58]

The quality of spectral unmixing results mainly depends on the spectral library. Unmixing techniques include Multiple Endmember Spectral Mixture Analysis (MESMA), Linear Spectral Mixture Model, Constrained Least Squares Linear Mixture Model, Unconstrained Linear Spectral Mixture Model, Mixture Tuned Matched Filtering Method, Constrained Linear Spectral Mixture Model and Monte Carlo Spectral Mixture Analysis (MCSMA).[59,60] The authors performed LU/LC classification for HSP images of Singapore and the coastal Jambi province on the island of Sumatra in Indonesia. Principal Component Analysis (PCA) along with the ISODATA classification method were used. Pixel unmixing was used to determine the abundance of each end member class.[61] An HSP image of Bangalore city was analysed using per-pixel classifiers like Spectral Angular Mapper (SAM) and SVM. Atmospheric effects in the HSP images were corrected using the Fast Line-of-sight Atmospheric Analysis of Hypercubes (FLAASH) module, and the authors reduced the dimensionality of the data with the Minimum Noise Fraction (MNF) transformation.[62] LU/LC classes were determined by SAM and SVM for HSP satellite data of the Kozhikode district, Kerala. The MODTRAN-based FLAASH module was used to correct the atmospheric effects and PCA provided the discrete reflectance values.[63]

In this review we summarise and explain the methods frequently used to analyse LU/LC change. Detailed review of LU/LC change analysis by other researchers has helped us by providing the questions below.

1) What are all the important LU/LC change application areas?
2) How and where to collect the data to analyse the LU/LC change for a particular area?
3) What geospatial software is available to process the satellite images?
4) What are the methods used for satellite image pre-processing?
5) What are the LU/LC classifications, clustering and spectral unmixing methods used by researchers?
6) What are all the performance metrics used by researchers to evaluate satellite images?
7) What are the landscape change models used for forecasting past, present and future LU/LC changes?

This review answers these questions to help future researchers in the field of remote sensing of the environment. The workflow of LU/LC change analysis is shown in Figure 1. This includes data acquisition of MSP and HSP satellite images, pre-processing of those satellite images, spectral analysis techniques, accuracy assessment using classified and ground truth data, and finally LU/LC change analysis. The rest of the review provides detailed information in sections on LU/LC applications and the study area selection, data acquisition, geospatial software tools, pre-processing techniques, some LU/LC classification and clustering methods, spectral unmixing techniques, landscape change models and evaluation metrics.

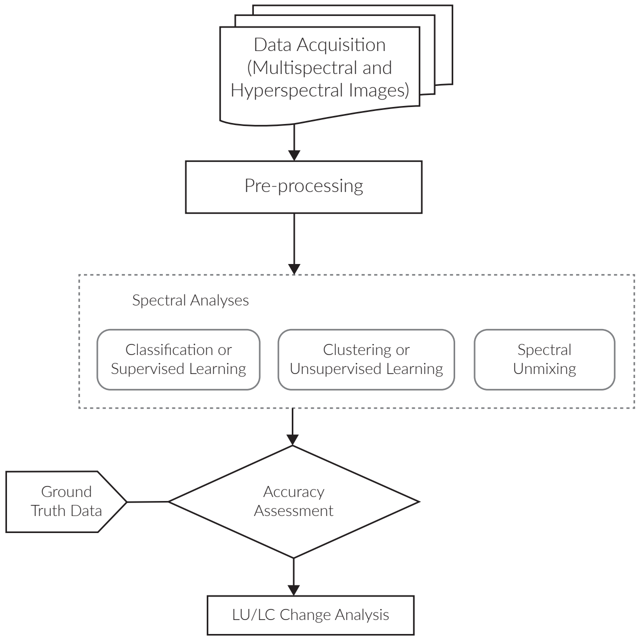

Figure 1. General flow of LU/LC change classification process.

LU/LC applications and study area selection

The modification of the Earth's surface or natural environment results in LU/LC change. We can see LU/LC change happening during the loss or development of forests, agricultural land, bodies of water and urban areas. Causes of LU/LC change are shown in Figure 2.

The initial process in LU/LC change research is selecting the study area. Many researchers around the world have carried out LU/LC change analysis research over many years. Some of the study areas for LU/LC analysis have been North-eastern Latvia,[1] Iranian Northern Zagros

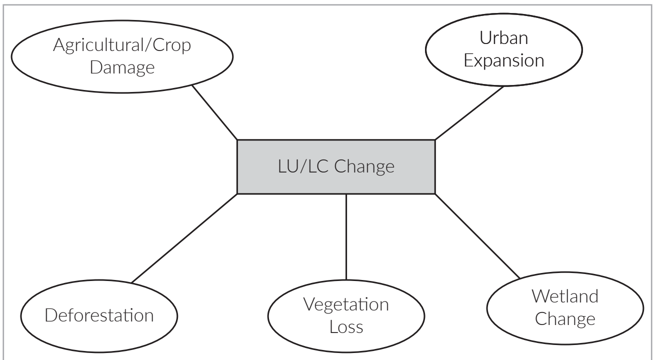

Figure 2. Causes of LU/LC.

forests,[7] Northern Ethiopia,[9] Mexico,[14] Germany,[18] China,[23] Iran,[25] Egypt,[27] United Arab Emirates,[31] India,[32] Iraq,[37] Malaysia,[41] south-western Australia,[44] Eastern Region of Ghana,[50] Dubai,[52] south-western Nigeria,[54] Indonesia,[55] Pakistan[56] and Sri Lanka.[57] The main objective of researchers in choosing their study area depends on the causes of LU/LC change (Figure 2), and their work assists government, forest departments, land resource and urban planners in taking the necessary actions to protect the Earth's environment.

Data acquisition

Information about the Earth's environment is collected through sources including aerial photographs, Google Maps, ground surveys and satellite images. The importance of working in the field of remote sensing lies in providing good resolution MSP and HSP satellite images. Satellite images are downloaded with datum coordinates in the GeoTIFF format. The satellite data are selected based on the study area. Time series data collected from different satellites have been used to study various examples of LU/LC. The researchers used many datasets to analyse LU/LC change, and Table 1 shows some of the datasets and their characteristics.

Geospatial software

MSP and HSP satellite images are analysed and processed through different geospatial software tools. Some of these tools are described in Table 2: ERDAS Imagine, Quantum GIS QGIS, IDRISI, ArcGIS, ENVI, Matlab, Python and Rstudio. Open-source software like Matlab, Python and Rstudio have an advantage for researchers in finding new algorithms to work with MSP and HSP satellite images. The QGIS geospatial software is also open-source, and it helps researchers to work efficiently with the HSP and MSP satellite images.

Table 1. Satellite image database and its characteristics.

Satellite image database	Spatial and spectral information			Purpose	Data source
	No. of bands/ band name	WL/CWL range	RL (m)		
Earth Observing-1 (EO-1)					
Advanced Land Imager (ALI)[64,65]	B1: Panchromatic	0.48–0.69 µm	10	The multispectral instrument helps to reduce the cost and size of the Landsat-type instruments. ALI's multispectral bands are similar to those of Landsat in many respects.	USGS: earthexplorer.usgs.gov
	B2: Blue	0.433–0.453 µm	30		
	B3: Blue	0.45–0.515 µm	30		
	B4: Green	0.525–0.605 µm	30		
	B5: Red	0.633–0.690 µm	30		
	B6: NIR	0.775–0.805 µm	30		
	B7: NIR	0.845–0.890 µm	30		
	B8: SWIR	1.20–1.30 µm	30		
	B9: SWIR	1.55–1.75 µm	30		
	B10: SWIR	2.08–2.35 µm	30		
Hyperspectral Imager Hyperion[61–63,65–67]	220 Bands	0.4–2.5 µm	30m	Helps to calibrate the high quality HSP satellite data that supports the evaluation of the Earth observing missions.	USGS: earthexplorer.usgs.gov
Linear etalon imaging spectrometer array Atmospheric Corrector (LAC)[65]	256 Bands	0.9–1.6 µm	250m	Atmospheric water absorption lines are monitored using LAC and it helps in correcting the atmospheric effects MSP satellite imagers on Landsat Enhanced Thematic Mapper ETM+.	
Resourcesat-1, Resourcesat-2					
Linear Imaging Self-Scanning Sensor (LISS-III)[32,34,36,40,42,46–48,53,62,66]	B2: Green	0.52–0.59 µm	23.5	Helps in analysing agricultural harvest monitoring, water resource consumption, forest mapping and rural/urban infrastructure expansion.	Bhuvan Indian Geo-Platform of ISRO: www.bhuvan.com
	B3: Red	0.62–0.68 µm	23.5		
	B4: NIR	0.77–0.86 µm	23.5		
	B4. SWIR	1.55–1.75 µm	23.5		

Landsat series					
Landsat 8–Operational Land Imager (OLI) and the Thermal Infrared (TI) Sensor[7,10,12–14, 16–19,22,23,25,26,35,37,40,44,49,52,54,68]	B1: Coastal/Aerosol	0.43–0.45 µm	30	Helps in analysing different kinds of LU/LC changes like deforestation, agriculture development, the evolution of built-up areas and loss of wetlands.	USGS: earthexplorer.usgs.gov
	B2: Blue	0.45–0.51 µm	30		
	B3: Green	0.53–0.59 µm	30		
	B4: Red	0.64–0.67 µm	30		
	B5: NIR	0.85–0.88 µm	30		
	B6: SWIR 1	1.57–1.65 µm	30		
	B7: SWIR 2	2.11–2.29 µm	30		
	B8: Panchromatic	0.50–0.68 µm	15		
	B9: Cirrus	1.36–1.38 µm	30		
	B10: TIRS 1	10.6- 11.19 µm	100		
	B11: TIRS 2	11.50–12.51 µm	100		
Landsat 7 ETM+ Sensor[4,6–9,11,13,14,16–18,22,24,28,30–32,35,43,44,52,54,57,64,68–76]	B1: Blue	0.45–0.52 µm	30		
	B2: Green	0.52–0.60 µm	30		
	B3: Red	0.63–0.69 µm	30		
	B4: NIR	0.77–0.90 µm	30		
	B5: SWIR 1	1.55–1.75 µm	30		
	B6: TIRS	10.40–12.50 µm	60		
	B7: SWIR 2	2.09–2.35 µm	30		
	B8: Panchromatic	0.52–0.90 µm	15		
Landsat 4 & Landsat 5 Multispectral Scanner (MSS) & Thematic Mapper (TM)[1,6–12,14–16,18,19,22–28,31,33,35–37,39,44,49,53,54,56–58,67–70,72–75,77–81]	B1: Blue	0.45–0.52 µm	30		
	B2: Green	0.52–0.60 µm	30		
	B3: Red	0.63–0.69 µm	30		
	B4: NIR	0.76–0.90 µm	30		
	B5: SWIR 1	1.55–1.75 µm	30		
	B6: TIRS	10.40–12.50 µm	120		
	B7: SWIR 2	2.08–2.35 µm	30		
Sentinel 2 missions					
Sentinel- 2A and 2B[13,18,20,51]	B1: Ultra blue Coastal and Aerosol	0.443 µm	60	Sentinel missions support the standard LU/LC change detection maps and help in finding leaf water and chlorophyll content.	Sentinel's Scientific Data Hub: scihub.copernicus.eu
	B2: Blue	0.490 µm	10		
	B3: Green	0.560 µm	10		
	B4: Red	0.665 µm	10		
	B5: Vegetation Red Edge	0.705 µm	20		
	B6: Vegetation Red Edge	0.740 µm	20		
	B7: Vegetation Red Edge	0.783 µm	20		
	B8: NIR	0.842 µm	10		
	B8a: Narrow NIR	0.865 µm	20		
	B9: Water Vapour	0.945 µm	60		
	B10: SWIR-Cirrus	1.375 µm	60		
	B11: SWIR	1.610 µm	20		
	B12: SWIR	2.190 µm	20		

Moderate Resolution Imaging Spectroradiometer (MODIS)					
NASA Terra and Aqua Satellite[2,17,69,75]	B1: Red	620–670 nm	250	MODIS data mainly reflect the activity that happens in the lower atmosphere and in the oceans.	Earth data: earthdata.nasa.gov/ USGS, earth-explorer.usgs.gov
	B2: NIR	841–876 nm	250		
	B3: Blue	459–479 nm	500		
	B4: Green	545–565 nm	500		
	B5: NIR	1230–1250 nm	500		
	B6: SWIR	1628–1652 nm	500		
	B7: SWIR	2105–2155 nm	500		
	B8: Ocean Colour	405–420 nm	1000		
	B9: Ocean Colour	438–448 nm	1000		
	B10: Ocean Colour	483–493 nm	1000		
	B11: Ocean Colour	526–536 nm	1000		
	B12: Ocean Colour	546–556 nm	1000		
	B13: Ocean Colour	662–672 nm	1000		
	B14: Ocean Colour	673–683 nm	1000		
	B15: Ocean Colour	743–753 nm	1000		
	B16: Ocean Colour	862–877 nm	1000		
	B17: Atmospheric Water Vapour	890–920 nm	1000		
	B18: Atmospheric Water Vapour	931–941 nm	1000		
	B19: Atmospheric Water Vapour	915–965 nm	1000		
	B20: Cloud Temperature	3.660–3.840 µm	1000		
	B21: Cloud Temperature	3.929–3.989 µm	1000		
	B22: Cloud Temperature	3.929–3.989 µm	1000		
	B23: Cloud Temperature	4.020–4.080 µm	1000		
	B24: Atmospheric Temperature	4.433–4.498 µm	1000		
	B25: Cloud Temperature	4.482–4.549 µm	1000		
	B26: Cirrus clouds water vapour	1.360–1.390 µm	1000		
	B27: Water Vapour	6.535–6.895 µm	1000		
	B28: Water Vapour	7.175–7.475 µm	1000		

	B29: Cloud Properties	8.400–8.700 µm	1000		
	B30: Ozone	9.580–9.880 µm	1000		
	B31: Cloud temperature	10.780–11.280 µm	1000		
	B32: Cloud temperature	11.770–12.270 µm	1000		
	B33: Cloud top altitude	13.185–13.485 µm	1000		
	B34: Cloud top Altitude	13.485–13.785 µm	1000		
	B35: Cloud top altitude	13.785–14.085 µm	1000		
	B36: Cloud top altitude	14.085–14.385 µm	1000		
Rapid Eye Earth Imaging System (REIS)					
RapidEye 1–TACHYS RAPID, RapidEye 2–MATI EYE, RapidEye 3–CHOMA EARTH, RapidEye 4–CHOROS SPACE, RapidEye 5–TROCHIA ORBIT[18]	B1: Blue	440–510 nm	5	The RapidEye satellite helps in providing continuous multitemporal time series data for a specific location.	ESA Earth Online: earth.esa.int
	B2: Green	520–590 nm	5		
	B3: Red	630–685 nm	5		
	B4: Red Edge	690–730 nm	5		
	B5: NIR	760–850 nm	5		
Quick Bird					
Ball Global Imaging System 2000 (BGIS-2000)[3,45,52,55,67,76]	B1: Blue	0.450-0.520 µm	2.4	Quick Bird acquires satellite imagery with high quality for creating land cover maps and land cover change detection.	Digital Globe: www.digital-globe.com
	B2: Green	0.520–0.600 µm	2.4		
	B3: Red	0.630–0.690 µm	2.4		
	B4: NIR	0.760–0.900 µm	2.4		
	B5: Panchromatic	0.450–0.900 µm	0.65		
Digital Elevation Model (DEM)					
ASTER Global DEM[1, 7–9,12,13,19–25,27,31,32,36,39,43,44,53,54,57,58,69,77,78]	B1: Green	0.520–0.60 µm	15	Terrain features like elevation, slope, aspect and surface temperature of land and emissivity are determined.	USGS: earthexplorer.usgs.gov
	B2: Red	0.630–0.690 µm	15		
	B3: NIR	0.760–0.860 µm	15		
	B4: NIR	0.760–0.860 µm	15		
	B5: SWIR	1.600–1.700 µm	30		
	B6: SWIR	2.145–2.185 µm	30		
	B7: SWIR	2.185–2.225 µm	30		
	B8: SWIR	2.235–2.285 µm	30		
	B9: SWIR	2.295–2.365 µm	30		
	B10: TIR	2.360–2.430 µm	30		
	B11: TIR	8.125–8.475 µm	90		
	B12: TIR	8.475–8.825 µm	90		
	B13: TIR	8.925–9.275 µm	90		
	B14: TIR	10.250–10.950 µm	90		

WL: wavelength, CWL: centre wavelength, RL: resolution, NIR: near infrared, SWIR: short wave infrared, TIRS: thermal infrared sensor

Table 2. Geospatial software.

<table>
<tr><th>Software</th><th>Source</th><th colspan="2">Purpose</th><th>Licence</th></tr>
<tr><td>Environment for Visualising Images (ENVI)[6,7,12,13,15–17,23,25,26,29,31,37,40,41,45–47,49,51,56,61–63,66]</td><td>Harris Geospatial Solutions: www.harrisgeospatial.com</td><td colspan="2">This software is used for MSP and HSP satellite image pre-processing, classification, clustering, spectral unmixing and calculating LU/LC change. Spectral band calculation for different sets of satellite data is performed.</td><td>Proprietary</td></tr>
<tr><td>ArcGIS[1,6,9,12,13,17,20–23,25,29,31–36,38–40,43,48,53–55,57,58,68,70,72,78]</td><td>Environmental Systems Research Institute (ESRI): www.esri.com/software/arcgis</td><td colspan="2">The primary purpose of this software is to work with MSP and HSP satellites for pre-processing, classification, clustering and LU/LC change detection.</td><td>Proprietary</td></tr>
<tr><td>IDRISI[6,7,13,14,22–27,31,35,39,53,55,58,68,76]</td><td>Clark Labs: clarklabs.org</td><td colspan="2">The primary purpose of this software is pre-processing, classification, clustering, modelling dependent and independent variables, and LU/LC change prediction can be made.</td><td>Proprietary</td></tr>
<tr><td>Earth Resources Data Analysis System (ERDAS IMAGINE)[1,22,24,29,30,32–36,39,54,58,62,68,70,72,76,78,79]</td><td>Hexagon Geospatial: www.hexagongeospatial.com</td><td colspan="2">This software performs pre-processing operations, classification, clustering and LU/LC change detection.</td><td>Proprietary</td></tr>
<tr><td>Quantum GIS (QGIS)[13,18,43,54]</td><td>QGIS Developers Team: qgis.org</td><td colspan="2">This software is used for performing pre-processing, post-processing, classification, prediction and for calibrating the terrain features.</td><td>General Public License</td></tr>
<tr><td>Matlab[2,11,46,50,72]</td><td>Math Works: www.mathworks.com</td><td colspan="2">This software is used for vector data representation, importing and exporting the geographic data. Matlab also performs map projections, coordinate transformations, web mapping, terrain and elevation analysis.</td><td>General Public License</td></tr>
<tr><td colspan="2"></td><th>Geospatial-libraries</th><th>Purpose</th><td></td></tr>
<tr><td rowspan="11">Python[10]</td><td rowspan="11">Python Software Foundation: www.python.org</td><td>Rasterio</td><td>Raster data handling</td><td rowspan="11">General Public License</td></tr>
<tr><td>Scikit-learn</td><td>Geospatial image classification, regression, dimensionality reductions etc.</td></tr>
<tr><td>Geospatial Data Abstraction Library (GDAL)</td><td>Geospatial data format conversion of raster and vector formats.</td></tr>
<tr><td>Fiona</td><td>Reads and writes geospatial data.</td></tr>
<tr><td>Shapely</td><td>Geometric calibration of geospatial data.</td></tr>
<tr><td>Geopandas</td><td>Geospatial Image Overlay, Geo-referencing.</td></tr>
<tr><td>Matplotlib</td><td>Plots 2D spatial data.</td></tr>
<tr><td>Remote Sensing and GIS Library (RSGSLib)</td><td>Object-based segmentation and classification on geospatial data.</td></tr>
<tr><td>Python Spatial Analysis Library (PySal)</td><td>Statistical modelling, spatial analysis and plotting.</td></tr>
<tr><td>Xarray</td><td>Geospatial image time series stacks handling.</td></tr>
<tr><td>PyProj</td><td>Functions coordinate reference system of each geospatial data.</td></tr>
</table>

Rstudio[44,49]	RStudio, Inc.: www.rstudio.com	Sp	Spatial data analysis	General Public License
		Rgdal	Read spatial data	
		raster	Raster data handling	
		ggplot2	Plots spatial data, spatial data visualisation.	
		viridis	Provides accessible colour palettes for spatial data.	
		rasterVis	Plotting	
		RStoolbox	Raster time series data	
		Caret	Classification and regression training of spatial data.	

Pre-processing techniques

Pre-processing is an essential technique used to improve the quality of raw satellite data. The satellite data can be calibrated by using the process of atmospheric, radiometric, geometric and topographic corrections. The uses and limitations of these methods are shown in Table 3. Researchers use image enhancement techniques to reduce the dimensionality of the satellite data: PCA, MNF, Independent Component Analysis (ICA) and wavelet dimensionality reduction.[9,19,25,29,30,34,46,47,51,53,54,56,61–63,67,80,82] Frequently used atmospheric correction methods are Dark Object Subtraction (DOS), Quick Atmospheric Correction (QUAC), FLAASH, Apparent Reflectance Model (ARM) and the F mask method.[7–9,12,15,18–20,23,28,29,33,35,37,40,41,45,49,61–63,66,67,70,74,75,79] Geometric corrections include Orthorectification, Geo-referencing, Image Registration, ASCII Coordinate Conversion and Resampling.[1,7,13,16,22–26,29,30,32–37,40,47–49,53,55,69,70,79] The Image De-striping, Rescaling, Point Spread Convolution and Lookup Table (LUT) Stretch methods have been used during radiometric correction.[9,13,22,23,26,29,40,41,44,47,49,70,71,79] Topographic corrections include normalise, level slicing, route intervisibility, surface difference and terrain elevation modelling of explanatory variables like slope, elevation and aspect etc.[12,23,25,29,35,37,40,74,77,79]

LU/LC classification and clustering

Every pixel in a pre-processed satellite image is a unique entity and it has to be labelled to obtain the LU/LC classification maps using different classification techniques. Researchers have proposed and worked with many algorithms for extracting LU/LC data from satellite data. Classification or supervised learning works with known information about the data and is used in classifying LU/LC classes. Clustering is used for unsupervised learning, since there is no prior information about the labelled data. A few LU/LC classifications, supervised and clustering unsupervised methods are explained and shown in Table 4.

Spectral unmixing

Spectral unmixing helps to identify pixels that contain more than one LU/LC type. The measured range of a mixed pixel is decomposed into a group of endmembers and their corresponding abundances, which specify the amount of each endmember within the pixel. Spectral unmixing methods are mostly used when processing HSP satellite images. The few spectral unmixing methods are explained and shown in Table 5.

Landscape change models

Landscape change models are used for forecasting past, current and future LU/LC changes. LU/LC change analysis results will assist urban planners in taking the necessary action to protect the LU/LC environment. Table 6 shows frequently used landscape change models. An often-used hybrid model for LU/LC change analysis is the MC-CA model.[5–7,13,14,22–27,31,33,35,53,55,58,74,78] The LCM is an innovative prediction tool frequently used by researchers for LU/LC change analysis. This simulation model in IDRISI software simulates the LU/LC change trends by using different methods like MC, MLP, LR and SimWeight, and

Table 3. Pre-processing techniques.

Techniques	Uses	Limitations
Image Enhancement[9,19,25,29,30,34,46,47,51,53,54,56,61–63,67,80,82]	This method helps in reducing the dimensionality and enhancing the contrast of the satellite image.	Information loss when compared to original satellite images.
Radiometric Correction[9,13,22,23,26, 29,40–42,47,49,70,71,79]	This method helps in the correction of digital number errors in the satellite image.	High computation time for larger datasets.
Atmospheric Correction[7–9,12,15,18–20,23,28,29,33,35,37,40,41,45,49,61–63,66,67,70,74,75,79]	This method helps to correct the atmospheric effects on the reflectance values of the satellite images.	Removing the whole cloud or atmospheric effects in a satellite image that was acquired during the winter season is not easy.
Geometric Correction[1,7,13,16,22–26, 29,30,32–37,40,47–49,53,55,69,70,79]	This method helps to correct the geometric distortions of a satellite image through the relationship between the Image Coordinate System (ICS) and Geographic Coordinate System (GCS).	Edges are flattened and some limits of the data pixel values will be lost.
Topographic Correction[12,23,25,29,35,37,40,74,77,79]	This method helps to correct the terrain radiance of the acquired topographic data.	Spatial misregistration can occur.

the modified K-nearest neighbour machine learning algorithm.[6,7,26,35,55] QGIS is an open-source tool that helps in analysing LU/LC changes across the world.[43,54]

Evaluation metrics

Researchers have used the information from satellite images to determine land cover. They used the spectral bands directly to identify the level of vegetation over the area and validated the LU/LC classified map with reference data. Distance metrics were used to identify the LU/LC class in satellite images through the evaluation of the spectral distance between the pixels. Researchers have also calculated the amount of LU/LC changes experienced between certain time periods.

Spectral distance metrics

By evaluating the spectral distance between the pixels in satellite images, LU/LC classes were assessed and this also helps to model spatial variables like slope, elevation, aspect, distance from the road, forest edge, farmland and water bodies etc. The frequently used distance metrics described in the following section are: Euclidean Distance, Mahalanobis Distance, Manhattan Distance, Canberra Distance, Jeffries–Matusita and SAM.

Euclidean Distance

Remote sensing researchers frequently use Euclidean Distance $d(x,y)$ to measure the distance between spectral signatures of satellite image pixels in n-dimensional spectral space.[42] This metric is used to model the independent variables based on the LU/LC map by calculating the distance map as distance from agricultural lands, forest edge, water bodies, built-up areas and roads.[7,29,36,39,55]

$$d(x,y)=\sqrt{\sum_{i=1}^{n}(x_i-y_i)^2} \tag{1}$$

where x and y represent the spectral signature vectors of image pixels and n represents the number of bands in the image.

Mahalanobis Distance

The Mahalanobis Distance classifier, which computes the Mahalanobis distance $D_i(x)$ between two data points in multivariate space is:[4,42,47]

Table 4. LU/LC classification and clustering.

Methods	Purpose	Limitations
Classification methods		
Maximum Likelihood Classification[1,4,7,9,12,13,15–17,22,23,25,26,30,32–37,39,40,42,47–49,51,54,55,57,68,70,80]	Estimation of each pixel to the LU/LC class which has the highest probability.	Increase in computation time when the number of bands of the satellite image increases.
k-Nearest Neighbour Classification (kNN)[4,20]	Statistical evaluation of satellite images to classify the nearest LU/LC class using the distance function.	With high dimensional data, the kNN algorithm performs a slower calculation of distance in each dimension.
SVM Classification[4,20,40,41,44,47,51,56,62,63,67]	This method helps to find the hyper-plane that separates two or more LU/LC classes in the satellite image.	The performance of SVM will be weak when the pixels of the satellite image are overlapped, i.e. when the satellite data are noisy.
ANN Classification[4–7,15,17,21,35,43,53,56,72,73]	The pixels in the satellite images are trained and separated into LU/LC classes through the learning process.	More massive datasets take a long time to train—time consuming.
Parallelepiped Classification[47,48,51]	The standard deviation threshold of each LU/LC class defined in the training data determines whether the pixel lies within the specific class type or not.	Problems occur when the class ranges are overlapped.
Minimum Distance to Mean Classification[42,47,48,51]	The LU/LC class defined by calculating the distance between the data points to their centroids.	Choosing the wrong number of clusters will lead to misclassification.
Mahalanobis Distance Classification[4,42,47]	The Mahalanobis distance is a direction-sensitive distance classification method that measures the statistics for every LU/LC class.	If the variables are highly correlated, misclassification will occur.
SAM Classification[41,52,62,63,66]	The LU/LC classes in the satellite image are identified based on calculation of the spectral angle.	Similar spectra are wrongly classified, for example, needle leaf and broadleaf forests are misclassified.
CART model		
Logistic Regression Model[5,6,36,38,39,55,68,78]	The logistic regression model helps to explain the association between dependent and independent variables.	Non-linear problems were difficult to solve with the logistic regression model.
Random Forest Classification[4,8,11,19,20,27,28,44]	LU/LC classification is performed based on the voting results of each decision tree.	Constructing decision trees consumes more time while performing Random Forest Classification.

MARS[11,73]	This model uses essential functions of the specific LU/LC class as predictors in place of the original satellite data.	The MARS method is not suitable when handling missing data.
CART[10,11,19,44]	The model is created by predicting the value of dependent variables based on the values of many independent variables.	Computational time is high to train every decision tree and tree structure is unstable when the data is changed.
Clustering methods		
K-Means Clustering[3,4,14,46,51]	The clusters of similar and dissimilar pixels are separated using the distance function.	The k-Means method does not perform well when the clusters are of different sizes.
Fuzzy C Means (FCM)[45,46,50,82]	The clustering method allows one pixel of a satellite image to belong to two or more clusters and helps in the minimisation of the objective function.	Computational time is high for more substantial dimensionality data.
ISODATA[4,22,31,36,44,46,49,51,61,76]	Based on the shortest distance between each cluster centre, the pixels of the satellite image are assigned to the nearest LU/LC class.	Computational time is high when the data is unstructured.

$$D_i(x) = \sqrt{(x-\mu_i)^T \sum_i^{-1} (x-\mu_i)} \tag{2}$$

where i represents the i^{th} class, x represents the number of bands of n-dimensional data, μ_i represents the mean vector of the class and Σ_i^{-1} represents the inverse covariance matrix of a class.

Manhattan and Canberra Distance

Manhattan Distance $D_M(x,y)$ computes the distance between the spectral values of the image pixel in a grid-like path.[2] Canberra Distance $D_C(x,y)$ is a weighted version of the Manhattan distance, and it measures the fraction difference between spectral values of the image pixel,[10]

$$D_M(x,y) = \sum_{i=1}^{n} |x_i - y_i| \tag{3}$$

$$D_C(x,y) = \sum_{i=1}^{n} \frac{|x_i - y_i|}{|x_i| + |y_i|} \tag{4}$$

where n is the number of bands, and x_i and y_j are the spectral values of the image pixel.

Jeffries–Matusita Distance

Both the Jeffries–Matusita Distance and transformed divergence[31,40] are used to calculate the separability between the class values and pixel values and it is expressed as

$$JM_{xy} = 2(1 - e^{-B}) \tag{5}$$

$$B = \frac{1}{8}(x-y)^t \left(\frac{\Sigma_x - \Sigma_y}{2}\right)^{-1} (x-y) + \frac{1}{2}\ln\left(\frac{\left|\frac{\Sigma_x + \Sigma_y}{2}\right|}{|\Sigma_x|^{\frac{1}{2}} |\Sigma_y|^{\frac{1}{2}}}\right) \tag{6}$$

where x represents the first spectral signature vector, y represents the second spectral signature vector, and Σ_x and Σ_y represent the covariance matrix of samples x and y.

Spectral angular mapper

The SAM, $\theta(x,y)$, differentiates the spectral similarity by measuring the angle between the spectral signatures of satellite image pixels and the training spectral signatures.[41,52]

Table 5. Spectral unmixing.

Methods	Purpose	Limitations
MESMA[59,60,75,76]	The possible combinations of two or more spectral endmembers are applied to each pixel for unmixing a satellite image.	The output will not be accurate when the given inputs have the wrong parameters and distributions.
Linear Spectral Mixture Model (LSMM)[59,60]	This method solves for the abundance fractions of each endmember of every mixed pixel in the satellite image.	The main limitation of LSMM is endmember variability.
Fully Constrained Least Squares (FCLS)[59,81]	This method efficiently meets the abundance constraints by discarding the negative abundance values in terms of least square error.	The image correction is not trivial and errors occur frequently.
Unconstrained Least Squares (UCLS)[59,60,81]	The abundances are estimated by least squares when all information about the endmembers and spectral signatures are known.	The low spatial resolution of the satellite image can lead to the most challenging problem of mixed pixels.
Mixture Tuned Matched Filtering (MTMF) Method[59,80]	Mixed filtering is used to reduce the false positive pixels in the satellite images.	The flexibility of the method can also be a drawback since, due to spectral variability, false detection may occur in mixed pixels of the satellite image.
Monte Carlo Spectral Mixture Analysis (MCSMA)[59,60]	Spectral data are randomly selected to calculate the two or more endmember mixtures of each pixel in the satellite image.	Computational time is high and there is a risk of false precision.

$$\theta(x,y) = \cos^{-1}\left(\frac{\sum_{i=1}^{n} x_i y_i}{\left(\sum_{i=1}^{n} x_i^2\right)^{\frac{1}{2}} \times \left(\sum_{i=1}^{n} y_i^2\right)^{\frac{1}{2}}}\right) \tag{7}$$

where x represents the spectral signature vector of an image pixel, y represents the spectral signature vector of a training area and n represents the number of satellite image bands.

Vegetation index metrics

Spectral information helps researchers to monitor the surface of the Earth and, therefore, provides the time series status of the land cover regions. The spectral features of vegetation help to gain information about the growth of plants and green areas throughout the world. The spatial resolution of each satellite spectrum differs, and Table 1 displays information about the spectral characteristics of each satellite. The vegetation range of the satellite typically reflects the green wavelength and absorbs the blue and red wavelengths. Near infrared (NIR) wavelengths strongly reflect the vegetation, and the SWIR wavelengths are highly absorbed by water. We have explained the most commonly used vegetation indices for measuring the level of vegetation and the water content in the specific land cover region: EVI, NDVI and Normalised Difference Water Index (NDWI). The optimised vegetation index or EVI is useful in computing the global vegetation greenness. It corrects the canopy background noise of the data and displays areas with more dense vegetation.[2]

$$EVI = G \times \frac{(NIR - RED)}{(NIR + C_1 \times RED - C_2 \times BLUE + L)} \tag{8}$$

where G represents the Gain factor, NIR represents the near infrared band, RED represents the red band and $BLUE$ the blue band. C_1, C_2 and L are the coefficients of aerosol resistance. The coefficient value of $L = 1$, $C_1 = 6$, $C_2 = 7.5$ and gain factor $G = 2.5$ were represented using the standard MODIS EVI algorithm.

Table 6. Landscape change models.

Landscape change models	Variables needed	Application/ software type	Purpose	Limitations
MC[5,6,13,14,22–27,31,33,53,58]	LU/LC maps of different time periods. Minimum two different time series maps.	Stand-alone/ module of IDRISI and QGIS	Helps to calculate the transition probabilities among LU/LC classes.	Spatial patterns are difficult to predict and thus it produces non-geospatial output.
CA[5,6,13,14,22–27,31,33,53,58]	LU/LC maps of different time periods. Minimum two different time series map and independent variables. Slope, elevation and distance from forest edge, road, water bodies, waste land, grass land and agricultural land maps.	Stand-alone/module of IDRISI and QGIS	Helps in the simulation of the complex processes in both spatial and temporal changing aspects.	It is difficult to combine changing social and economic aspects during the simulation process.
GeoMod[12,53,58]	LU/LC maps of different time periods. Minimum two different time series map and spatial driver maps like slope, elevation, distance from forest edge, road, water bodies, waste land, grass land, and agricultural land maps.	IDRISI component	This method simulates the spatial change between the LU/LC categories for past, present and future time series data.	Data sets should be large, but then the computational cost is high and processing time long.
LCM[6,7,26,35,55]	Minimum two LU/LC maps and the spatial variables. Slope, elevation and distance from forest edge, road, water bodies, waste land, grass land and agricultural land maps.	IDRISI, ArcGIS V.10.2 and above	LCM is a land resource planning system that rapidly analyses future LU/LC change.	High computation time in modelling more spatial drivers.

Conversion of Land Use and its Effects (CLUE) model[5,6,78]	Spatial and non-spatial. Socio–economic variables, regional spatial variables and land-adaptive variables.	Stand-alone model	This model used in the spatial allocation of LU/LC changes.	Cannot directly be applied at the regional scale.
Modules for land use Change Evaluation (MOLUSCE)[43,54]	Actual LU/LC maps. Only two different years and spatial variables. Slope, aspect, hill shade and distance from forest edge, road, water bodies, waste land, grass land and agricultural land maps.	QGIS Plugin, minimum V.2.0.0	MOLUSCE performs fast and suitable analysis of LU/LC changes.	No precise declaration on when the bugs in the code will be corrected.

The high and low possibilities of vegetation are identified by using NDVI values.[8,10,18,26,44,46,70,72] NDVI values lie between –1 and +1.

$$NDVI = \frac{(NIR - RED)}{(NIR + RED} \tag{9}$$

The high and low possibilities of having water content are identified by NDWI values.[10,19,46] NDWI values lie between –1 and +1.

$$NDWI = \frac{(NIR - SWIR)}{(NIR + SWIR} \tag{10}$$

Classification metrics

The most important metric for validating LU/LC classification results is accuracy assessment. The accuracy of the LU/LC classified map is assessed by creating random point locations with their class value from the ground truth/reference data and by validating that with the classified data in a confusion matrix. The overall accuracy and the kappa coefficient are computed to validate the LU/LC classified result.[1,3,4,7–10,12–17,19,20,22,23,25–28,30–51,53–57,62,63,66–68,70,72,73,80] Table 7 illustrates the error matrix.

$$OA = \left(\frac{TP + TN}{N}\right) \times 100 \tag{11}$$

Table 7. Error matrix.

Classified Data (CD)	Reference Data (RD)	
	Positive	Negative
Positive	True Positive (TP)	False Negative (FN)
Negative	False Positive (FP)	True Negative (TN)

$$KC = \frac{N\sum_{i=1}^{r} x_{ii} \sum_{i=1}^{r}\left(x_{i+} \times x_{+i}\right)}{N^{2-} \sum_{i=1}^{r}\left(x_{i+} \times x_{+i}\right)} \tag{12}$$

Precision[2] is measured by using the correctly classified data True Positive with the overall referenced data False Positive and True Positive of the positive class. Recall[2] is measured by using the correctly classified data True Positive with the overall classified data True Positive and False Negative of the positive class. The F-Score[2] considers the both *PN* and *RL* and it is measured by calculating the *HM* harmonic mean between them.

$$Precision\ PN = \frac{TP}{(TP + FP)} \tag{13}$$

$$Recall\ RL = \frac{TP}{(TP + FN)} \tag{14}$$

$$F - Score = 2 \times \left(\frac{PN \times RL}{PN + RL} \right) \tag{15}$$

where OA represents overall accuracy, KC represents the kappa coefficient, N signifies the matrix total observations, r signifies the number of rows in the error matrix, x_{ii} denotes row i and column i observations, x_{i+} denotes row i observations and x_{+i} represents column i observations.

LU/LC change metrics

The rate and percentage of change are calculated to analyse the LU/LC change.[22]

$$POC = \left(\frac{TI_2 - TI_1}{TI_1} \right) \times 100 \tag{16}$$

$$ROC\ (\text{ha/yr}) = \frac{TI_1 - TI_2}{TI_i} \tag{17}$$

where POC represents the percentage of change, ROC represents the rate of change, TI_1 represents the area (ha) of LU/LC for time interval 1, TI_2 represents the area (ha) of LU/LC for time interval 2 and TI_i is the time interval between TI_1 and TI_2 in years.

Conclusion

In this paper, we have provided a review of the LU/LC change analysis process and the methods frequently used by researchers to analyse MSP and HSP satellite images. LU/LC change has been explained for various application areas such as deforestation, urban expansion, agriculture/crop damage, vegetation loss and wetland change. This review provides detailed information about the characteristics of satellite data, geospatial software, pre-processing techniques, classification, clustering and spectral unmixing methods, landscape change models and the performance metrics for evaluating the satellite images. Amongst geospatial software, Matlab, Python and Rstudio have the advantage in developing new algorithms for analysing LU/LC changes using HSP and MSP satellite images. Pre-processing should be performed to correct the geometric, radiometric, topographic and atmospheric effects present in satellite images. Classification, clustering and spectral unmixing methods are used to extract the spectral features from satellite images. Effective landscape models were used to analyse the LU/LC change for specific time intervals in a particular region. The importance of performance metrics has been discussed in this review. It should help future researchers to work on the LU/LC change analysis process in the field of remote sensing. Developing a new optimised algorithm for LU/LC classification and for analysing LU/LC change remains a challenge for future researchers. Information about LU/LC change will help to assist Government officials responsible for land resource planning to take adequate measures to protect the LU/LC environment.

Acknowledgement

We are grateful to the Vellore Institute of Technology for providing a VIT Seed Grant to carry out this review work.

References

1. S.F. Fonji and G.N. Taff, "Using satellite data to monitor land-use land-cover change in North-eastern Latvia", *SpringerPlus* **3,** 61 (2014). https://doi.org/10.1186/2193-1801-3-61
2. S. Panigrahi, K. Verma and P. Tripathi, "Data mining algorithms for land cover change detection: a review", *Sādhanā* **42,** 2081–2097 (2017). https://doi.org/10.1007/s12046-017-0751-4
3. B. Usman, "Satellite imagery land cover classification using k-means clustering algorithm computer vision for environmental information extraction", *Elixir Computer Science and Engineering* **63,** 18671–18675 (2013).
4. M. Li, S. Zang, B. Zhang, S. Li and C. Wu, "A review of remote sensing image classification techniques: The role of spatio-contextual information," *Eur. J. Remote Sens.* **47,** 389–411 (2014). https://doi.org/10.5721/EuJRS20144723
5. O. Bounouh, H. Essid and I.R. Farah, "Prediction of land use/land cover change methods: A study", *2017 International Conference on Advanced Technologies for Signal and Image Processing (ATSIP)*. IEEE (2017). https://doi.org/10.1109/ATSIP.2017.8075511
6. C. Nwaogu, A. Benc and V. Pechanec, "Prediction models for landscape development in GIS", in Dynamics in GIscience. GIS OSTRAVA 2017, Ed by I. Ivan, J. Horák and T. Inspektor. Lecture Notes in Geoinformation and Cartography. Springer, Cham

(2017). https://doi.org/10.1007/978-3-319-61297-3_21

7. H.B. Heidarlou, A.B. Shafiei, M. Erfanian, A. Tayyebi and A. Alijanpour, "Effects of preservation policy on land use changes in Iranian Northern Zagros forests", *Land Use Policy* **81,** 76–90 (2019). https://doi.org/10.1016/j.landusepol.2018.10.036
8. Q. Yang, H. Zhang, W. Peng, Y. Lan, S. Luo, J. Shao, D. Chen and G. Wang, "Assessing climate impact on forest cover in areas undergoing substantial land cover change using Landsat imagery", *Sci. Tot. Environ.* **659,** 732–745 (2019). https://doi.org/10.1016/j.scitotenv.2018.12.290
9. E. Birhane, H. Ashfare, A.A. Fenta, H. Hishe, M.A. Gebremedhin, H.G. Wahed and N. Solomon, "Land use land cover changes along topographic gradients in Hugumburda national forest priority area, Northern Ethiopia", *Remote Sens. Appl. Soc. Environ.* **13,** 61–68 (2019). https://doi.org/10.1016/j.rsase.2018.10.017
10. Y. Hu, Y. Dong and Batunacun, "An automatic approach for land-change detection and land updates based on integrated NDVI timing analysis and the CVAPS method with GEE support", *ISPRS J. Photogramm. Remote Sens.* **146,** 347–359 (2018). https://doi.org/10.1016/j.isprsjprs.2018.10.008
11. M. Ahmadlou, M.R. Delavar, A. Basiri and M. Karimi, "A comparative study of machine learning techniques to simulate land use changes", *J. Indian Soc. Remote Sens.* **47,** 53–62 (2019). https://doi.org/10.1007/s12524-018-0866-z
12. A.M. Cadavid Restrepo, Y.R. Yang, N.A.S. Hamm, D.J. Gray, T.S. Barnes, G.M. Williams, R.J. Soares Magalhães, D.P. McManus, D. Guo and A.C.A. Clements, "Land cover change during a period of extensive landscape restoration in Ningxia Hui Autonomous Region, China", *Sci. Tot. Environ.* **598,** 669–679 (2017). https://doi.org/10.1016/j.scitotenv.2017.04.124
13. A. El Jazouli, A.Barakat, R. Khellouk, J. Rais and M. El Baghdadi, "Remote sensing and GIS techniques for prediction of land use land cover change effects on soil erosion in the high basin of the Oum Er Rbia River (Morocco)", *Remote Sens. Appl. Soc. Environ.* **13,** 361–374 (2019). https://doi.org/10.1016/j.rsase.2018.12.004
14. R. Hernández-Guzmán, A. Ruiz-Luna and C. González, "Assessing and modelling the impact of land use and changes in land cover related to carbon storage in a western basin in Mexico", *Remote Sens. Appl. Soc. Environ.* **13,** 318–327 (2019). https://doi.org/10.1016/j.rsase.2018.12.005
15. H. Bagan, H. Li, Y. Yang, W. Takeuchi and Y. Yamagata, "Sensitivity of the subspace method for land cover classification", *Egypt. J. Remote Sens. Space Sci.* **21(3),** 383–389 (2018). https://doi.org/10.1016/j.ejrs.2017.12.003
16. N. Bakr and A.A. Afifi, "Quantifying land use/land cover change and its potential impact on rice production in the Northern Nile Delta, Egypt", *Remote Sens. Appl. Soc. Environ.* **13,** 348–360 (2019). https://doi.org/10.1016/j.rsase.2018.12.002
17. Z. Li, H. Bagan and Y. Yamagata, "Analysis of spatiotemporal land cover changes in Inner Mongolia using self-organizing map neural network and grid cells method", *Sci. Tot. Environ.* **636,** 1180–1191 (2018). https://doi.org/10.1016/j.scitotenv.2018.04.361
18. N. Kabisch, P. Selsam, T. Kirsten, A. Lauschf and J. Bumberger, "A multi-sensor and multi-temporal remote sensing approach to detect land cover change dynamics in heterogeneous urban landscapes", *Ecol. Indic.* **99,** 273–282 (2019). https://doi.org/10.1016/j.ecolind.2018.12.033
19. H.A. Zurqani, C.J. Post, E.A. Mikhailova, M.A. Schlautman and J.L. Sharp, "Geospatial analysis of land use change in the Savannah River Basin using Google Earth Engine", *Int. J. Appl. Earth Observ. Geoinform.* **69,** 175–185 (2018). https://doi.org/10.1016/j.jag.2017.12.006
20. P.T. Noi and M. Kappas, "Comparison of random forest, k-nearest neighbor, and support vector machine classifiers for land cover classification using Sentinel-2 imagery", *Sensors* **18(1),** 18 (2018). https://doi.org/10.3390/s18010018
21. C. Zhang, I. Sargent, X. Pan, H. Li, A. Gardiner, J. Hare and P.M. Atkinson, "Joint deep learning for land cover and land use classification", *Remote Sens. Environ.* **221,** 173–187 (2019). https://doi.org/10.1016/j.rse.2018.11.014
22. T. Gashaw, T. Tulu, M. Argaw and A.W. Worqlul, "Evaluation and prediction of land use/land cover changes in the Andassa watershed, Blue Nile Basin, Ethiopia", *Environ. Syst. Res.* **6,** 17 (2017). https://doi.org/10.1186/s40068-017-0094-5

23. C. Liping, S. Yujun and S. Saeed, "Monitoring and predicting land use and land cover changes using remote sensing and GIS techniques—A case study of a hilly area, Jiangle, China", *PLOS ONE* **13(7),** e0200493 (2018). https://doi.org/10.1371/journal.pone.0200493

24. S.K. Singh, Sk. Mustak, P.K. Srivastava, S. Szabó and T. Islam, "Predicting spatial and decadal LULC changes through cellular automata Markov chain models using Earth observation datasets and geo-information", *Environ. Process.* **2,** 61–78 (2015). https://doi.org/10.1007/s40710-015-0062-x

25. H. Karimi, J. Jafarnezhad, J. Khaledi and P. Ahmadi, "Monitoring and prediction of land use/land cover changes using CA-Markov model: a case study of Ravansar County in Iran", *Arab. J. Geosci.* **11,** 592 (2018). https://doi.org/10.1007/s12517-018-3940-5

26. H. Etemadi, J.M. Smoak and J. Karami, "Land use change assessment in coastal mangrove forests of Iran utilizing satellite imagery and CA–Markov algorithms to monitor and predict future change", *Environ. Earth Sci.* **77,** 208 (2018). https://doi.org/10.1007/s12665-018-7392-8

27. M.W.A. Halmy, P.E. Gessler, J.A. Hicke and B.B. Salem, "Land use/land cover change detection and prediction in the north-western coastal desert of Egypt using Markov-CA", *Appl. Geogr.* **63,** 101–112 (2015). https://doi.org/10.1016/j.apgeog.2015.06.015

28. Z. Zhu and C.E. Woodcock, "Continuous change detection and classification of land cover using all available Landsat data", *Remote Sens. Environ.* **144,** 152–171 (2014). https://doi.org/10.1016/j.rse.2014.01.011

29. D. Phiri and J. Morgenroth, "Developments in Landsat land cover classification methods: A review", *Remote Sens.* **9(9),** 967 (2017). https://doi.org/10.3390/rs9090967

30. P.S. Sisodia, V. Tiwari and A. Kumar, "Analysis of supervised maximum likelihood classification for remote sensing image", *International Conference on Recent Advances and Innovations in Engineering (ICRAIE-2014), Jaipur, 2014.* IEEE, pp. 1–4 (2014). https://doi.org/10.1109/ICRAIE.2014.6909319

31. M.M. Yagoub and A.A. Al Bizreh, "Prediction of land cover change using Markov and cellular automata models: case of Al-Ain, UAE, 1992-2030", *J. Indian Soc. Remote Sens.* **42,** 665–671 (2014). https://doi.org/10.1007/s12524-013-0353-5

32. C.B. Pande, K.N. Moharir, S.F.R. Khadri and S. Patil, "Study of land use classification in an arid region using multispectral satellite images", *Appl. Water Sci.* **8,** 123 (2018). https://doi.org/10.1007/s13201-018-0764-0

33. E. Yirsaw, W. Wu, X. Shi, H. Temesgen and B. Bekele, "Land use/land cover change modeling and the prediction of subsequent changes in ecosystem service values in a coastal area of China, the Su-Xi-Chang Region", *Sustainability* **9(7),** 1204 (2017). https://doi.org/10.3390/su9071204

34. P.K. Mallupattu and J.R.S. Reddy, "Analysis of land use/land cover changes using remote sensing data and GIS at an Urban Area, Tirupati, India", *Sci. World J.* **2013,** 268623 (2013). https://doi.org/10.1155/2013/268623

35. J. John, N.R. Chithra and SG. Thampi, "Prediction of land use/cover change in the Bharathapuzha river basin, India using geospatial techniques", *Environ. Monit. Assess.* **191,** 354 (2019). https://doi.org/10.1007/s10661-019-7482-4

36. S. Adhikari, T. Fik and P. Dwivedi, "Proximate causes of land-use and land-cover change in Bannerghatta National Park: a spatial statistical model", *Forests* **8(9),** 342 (2017). https://doi.org/10.3390/f8090342

37. K. Alkaradaghi, S.S. Ali, N. Al-Ansari and J. Laue, "Evaluation of land use & land cover change using multi-temporal Landsat imagery: a case study Sulaimaniyah Governorate, Iraq", *J. Geogr. Inform. Sys.* **10(3),** 247–260 (2018). https://doi.org/10.4236/jgis.2018.103013

38. H. Hemasinghe, R.S.S. Rangali, N.L. Deshapriya and L. Samarakoon, "Landslide susceptibility mapping using logistic regression model (a case study in Badulla District, Sri Lanka)", *Procedia Eng.* **212,** 1046–1053 (2018). https://doi.org/10.1016/j.proeng.2018.01.135

39. R. Kumar, S. Nandy, R. Agarwal and S.P.S. Kushwaha, "Forest cover dynamics analysis and prediction modelling using logistic regression model", *Ecol. Indic.* **45,** 444–455 (2014). https://doi.org/10.1016/j.ecolind.2014.05.003

40. M. Firoozynejad and A.A. Torahi, "Evaluation of IRS1D-LISS-III and Landsat 8-OLI images for mapping in Maroon Riparian Forest", *J. Geogr. Nat. Disast.*

7(2), 198 (2017). https://doi.org/10.4172/2167-0587.1000198

41. N.S.N. Shaharum, H.Z.M. Shafri, J. Gambo and F.A.Z. Abidin, "Mapping of Krau Wildlife Reserve (KWR) protected area using Landsat 8 and supervised classification algorithms", *Remote Sens. Appl. Soc. Environ.* **10,** 24–35 (2018). https://doi.org/10.1016/j.rsase.2018.01.002

42. K.O. Murtaza and S.A. Romshoo, "Determining the suitability and accuracy of various statistical algorithms for satellite data classification", *Int. J. Geomat. Geosci.* **4(4),** 585 (2014).

43. M.H. Saputra and H.S. Lee, "Prediction of land use and land cover changes for North Sumatra, Indonesia, using an artificial-neural-network-based cellular automaton", *Sustainability* **11(11),** 3024 (2019). https://doi.org/10.3390/su11113024

44. T. Nery, R. Sadler, M.S. Aulestia, B. White and M. Polyakov, "Discriminating native and plantation forests in a Landsat time-series for land use policy design", *Int. J. Remote Sens.* **40(11),** 4059–4082 (2019). https://doi.org/10.1080/01431161.2018.1558375

45. Y. HongLei, P. JunHuan, X. BaiRu and Z. DingXuan, "Remote sensing classification using fuzzy C-means clustering with spatial constraints based on Markov random field", *Eur. J. Remote Sens.* **46(1),** 305–316 (2013). https://doi.org/10.5721/EuJRS20134617

46. A. Taufik, S.S.S. Ahmad and E.F. Azmi, "Classification of Landsat 8 satellite data using unsupervised methods", in *Intelligent and Interactive Computing*. Lecture Notes in Networks and Systems, vol. 67, Ed by V. Piuri, V. Balas, S. Borah and S.S. Ahmad. Springer, Singapore, pp. 275–284 (2019). https://doi.org/10.1007/978-981-13-6031-2_46

47. A.D. Vibhute, A.D. Nagne, B.W. Gawali and S.C. Mehrotra, "Comparative analysis of different supervised classification techniques for spatial land use/land cover pattern mapping using RS and GIS", *Int. J. Sci. Eng. Res.* **4(7),** 1938–1946 (2013).

48. B.P. Ganasri and G.S. Dwarakish, "Study of land use/land cover dynamics through classification algorithms for Harangi catchment area, Karnataka State, India", *Aquatic Procedia* **4,** 1413–1420 (2015). https://doi.org/10.1016/j.aqpro.2015.02.183

49. K. Asubonteng, K. Pfeffer, M. Ros-Tonen, J. Verbesselt and I. Baud, "Effects of tree-crop farming on land-cover transitions in a mosaic landscape in the eastern region of Ghana", *Environ. Manage.* **62,** 529–547 (2018). https://doi.org/10.1007/s00267-018-1060-3

50. M.J. Khan, A. Yousaf, K. Khurshid, A. Abbas and F. Shafait, "Automated forgery detection in multispectral document images using fuzzy clustering", *2018 13th IAPR International Workshop on Document Analysis Systems (DAS), Vienna, 2018*. IEEE, pp. 393–398 (2018). https://doi.org/10.1109/DAS.2018.26

51. K.N. Priyadarshini, M. Kumar, S.A. Rahaman and S. Nitheshnirmal, "A comparative study of advanced land use/land cover classification algorithms using Sentinel-2 data", *Int. Arch. Photogramm. Remote Sens. Spatial Inf. Sci.* **XLII-5,** 665–670 (2018). https://doi.org/10.5194/isprs-archives-XLII-5-665-2018

52. M.M. Mohamed and S. Elmahdy, "Land use/land cover changes monitoring and analysis of Dubai Emirate, UAE using multi-temporal remote sensing data", *EPiC Ser. Eng.* **3,** 1435–1443 (2018).

53. M.A. Nadoushan, A. Soffianian and A. Alebrahim, "Predicting urban expansion in Arak Metropolitan Area using two land change models", *World Appl. Sci. J.* **18,** 1124–1132 (2012).

54. E.D. Ashaolu, J.F. Olorunfemi and I.P. Ifabiyi, "Assessing the spatio-temporal pattern of land use and land cover changes in Osun Drainage Basin, Nigeria", *J. Environ. Geogr.* **12(1–2),** 41–50 (2019). https://doi.org/10.2478/jengeo-2019-0005

55. A. Achmad, S. Hasyim, B. Dahlan and D.N. Aulia, "Modeling of urban growth in tsunami-prone city using logistic regression: analysis of Banda Aceh, Indonesia", *Appl. Geogr.* **62,** 237–246 (2015). https://doi.org/10.1016/j.apgeog.2015.05.001

56. A.W. Shahab-Ul-Islam, A.W. Abbas, A. Ahmad, S. Shah and K. Saeed, "Parameter investigation of artificial neural network and support vector machine for image classification", *2017 14th International Bhurban Conference on Applied Sciences and Technology (IBCAST), Islamabad, 2017*, pp. 795–798 (2017). https://doi.org/10.1109/IBCAST.2017.7868146

57. I.S.S. Pathiranage, L.N. Kantakumar and S. Sundaramoorthy, "Remote sensing data and SLEUTH urban growth model: as decision support tools for urban planning", *Chin. Geogr. Sci.* **28,** 274–286 (2018). https://doi.org/10.1007/s11769-018-0946-6

58. R. Regmi, S. Saha and M. Balla, "Geospatial analysis of land use land cover change predictive modeling at Phewa Lake Watershed of Nepal", *Int. J. Curr. Eng. Tech.* **4,** 2617–2627 (2014).

59. C. Quintano, A. Fernández-Manso, Y.E. Shimabukuro and G. Pereira, "Spectral unmixing", *Int. J. Remote Sens.* **33(17),** 5307–5340 (2012). https://doi.org/10.1080/01431161.2012.661095

60. R.A. Borsoi, T. Imbiriba, J.C.M. Bermudez, C. Richard, J. Chanussot, L. Drumetz, J.-Y. Tourneret, A. Zare and C. Jutten, "Spectral variability in hyperspectral data unmixing: a comprehensive review", arXiv:2001.07307 (2020). https://arxiv.org/abs/2001.07307

61. S.C. Liew, C.W. Chang and K.H. Lim, "Hyperspectral land cover classification of EO-1 Hyperion data by principal component analysis and pixel unmixing", *IEEE International Geoscience and Remote Sensing Symposium, Toronto, Ontario, Canada, 2002*, pp. 3111–3113, Vol. 6 (2002). https://doi.org/10.1109/IGARSS.2002.1027101

62. G. Hegde, J.M. Ahamed, R. Hebbar and U. Raj, "Urban land cover classification using hyperspectral data", *Int. Arch. Photogramm. Remote Sens. Spatial Inf. Sci.* **XL-8,** 751–754 (2014). https://doi.org/10.5194/isprsarchives-XL-8-751-2014

63. G. Gopinath, N. Sasidharan and U. Surendran, "Landuse classification of hyperspectral data by spectral angle mapper and support vector machine in humid tropical region of India", *Earth Sci. Inform.* 1–8 (2020). https://doi.org/10.1007/s12145-019-00438-4

64. A.J. Elmore and J.F. Mustard, "Precision and accuracy of EO-1 Advanced Land Imager (ALI) data for semiarid vegetation studies", *IEEE Trans. Geosci. Remote Sens.* **41(6),** 1311–1320 (2003). https://doi.org/10.1109/TGRS.2003.813132

65. M.A. Folkman, J. Pearlman, L.B. Liao and P.J. Jarecke, "EO-1/Hyperion hyperspectral imager design, development, characterization, and calibration", *Proc. SPIE 4151, Hyperspectral Remote Sensing of the Land and Atmosphere* (2001). https://doi.org/10.1117/12.417022

66. D. Vijayan, G.R. Shankar and T.R. Shankar, "Hyperspectral data for land use/land cover classification", *Int. Arch. Photogramm. Remote Sens. Spatial Inf. Sci.* **XL-8,** 991–995 (2014). https://doi.org/10.5194/isprsarchives-XL-8-991-2014

67. G. Mallinis, G. Galidaki and I. Gitas, "A comparative analysis of EO-1 Hyperion, Quickbird and Landsat TM imagery for fuel type mapping of a typical Mediterranean landscape", *Remote Sens.* **6(2),** 1684–1704 (2014). https://doi.org/10.3390/rs6021684

68. A. Nurwanda, A.F.M. Zain and E. Rustiadi, "Analysis of land cover changes and landscape fragmentation in Batanghari Regency, Jambi Province", *Procedia Social Behav. Sci.* **227,** 87–94 (2016). https://doi.org/10.1016/j.sbspro.2016.06.047

69. R.E. Wolfe, G. Lin, M. Nishihama, K.P. Tewari, J.C. Tilton and A.R. Isaacman, "Suomi NPP VIIRS prelaunch and on-orbit geometric calibration and characterization", *J. Geophys. Res. Atmosph.* **118(20),** 11,508–11,521 (2013). https://doi.org/10.1002/jgrd.50873

70. S. Das, M.R. Choudhury and S. Nanda, "Geospatial assessment of agricultural drought: a case study of Bankura District, West Bengal", *Int. J. Agric. Sci. Res.* **3(2),** 1–28 (2013).

71. F. Tsai and W.W. Chen, "Striping noise detection and correction of remote sensing images", *IEEE Trans. Geosci. Remote Sens.* **46(12),** 4122–4131 (2008). https://doi.org/10.1109/TGRS.2008.2000646

72. S. Kusuma, "Artificial neural network model for prediction of land surface temperature from land use/cover images", *Int. J. Adv. Trends Comput. Sci. Eng.* **2,** 87–92 (2013).

73. M. Ahmadlou, M.R. Delavar, A. Tayyebi and H. Shafizadeh-Moghadam, "Using multivariate adaptive regression spline and artificial neural network to simulate urbanization in Mumbai, India", *Int. Arch. Photogramm. Remote Sens. Spatial Inf. Sci.* **XL-1/W5,** 31–36 (2015). https://doi.org/10.5194/isprsarchives-XL-1-W5-31-2015

74. J. Mirkatouli, A. Hosseini and A. Neshat, "Analysis of land use and land cover spatial pattern based on Markov chains modelling", *City Territ. Archit.* **2,** 4 (2015). https://doi.org/10.1186/s40410-015-0023-8

75. M. Gan, J. Deng, X. Zheng, Y. Hong and K. Wang, "Monitoring urban greenness dynamics using multiple endmember spectral mixture analysis", *PLOS ONE* **9(11),** e112202 (2014). https://doi.org/10.1371/journal.pone.0112202

76. S.W. Myint and G.S. Okin, "Modelling land-cover types using multiple endmember spectral mixture analysis in a desert city", *Int. J. Remote Sens.* **30(9),** 2237–2257 (2009). https://doi.org/10.1080/01431160802549328

77. H.-p. Qin, W.-n. Yi, J.-j. Ma, X.-x. Ding and X.-b. Zhu, "Topographic imaging simulation of optical remote sensing based on Landsat TM data", *Optik* **124(7),** 586–589 (2013). https://doi.org/10.1016/j.ijleo.2011.12.058

78. H. Han, C. Yang and J. Song, "Scenario simulation and the prediction of land use and land cover change in Beijing, China", *Sustainability* **7(4),** 4260–4279 (2015). https://doi.org/10.3390/su7044260

79. S.S. Baboo and M.R. Devi, "Geometric correction in recent high resolution satellite imagery: a case study in Coimbatore, Tamil Nadu", *Int. J. Comput. Appl.* **14(1),** 32–37 (2011). https://doi.org/10.5120/1808-2324

80. S.G. Mehr, V. Ahadnejad, R.A. Abbaspour and M. Hamzeh, "Using the mixture-tuned matched filtering method for lithological mapping with Landsat TM5 images", *Int. J. Remote Sens.* **34(24),** 8803–8816 (2013). https://doi.org/10.1080/01431161.2013.853144

81. U. Kumar, C. Milesi, R.R. Nemani, S.K. Raja, W. Wang and S. Ganguly, "Partially and fully constrained least squares linear spectral mixture model for subpixel land cover classification using Landsat data", *Int. J. Sig. Proc. Sys.* **4(3),** 245–251 (2016). https://doi.org/10.18178/ijsps.4.3.245-251

82. S.N. Rehman and M.A. Hussain, "Fuzzy C-means algorithm based satellite image segmentation", *Indonesian J. Elec. Eng. Comput. Sci.* **9(2),** 332–334 (2018). https://doi.org/10.11591/ijeecs.v9.i2.pp332-334